Helmholtz-Zentrum Dresden-Rossendorf (HZDR)

HELMHOLTZ ZENTRUM
DRESDEN ROSSENDORF

SiCxNy:Fe films as a tunable ferromagnetic material with tailored conductivity

Pushkarev, R.; Fainer, N.; Kirienko, V.; Matsynin, A.; Nadolinnyy, V.; Merenkov, I.; Trubina, S.; Ehrenburg, S.; Kvashnina, K.;

Originally published:

March 2019

Journal of Materials Chemistry C 7(2019), 4250-4258

DOI: https://doi.org/10.1039/C9TC00299E

Perma-Link to Publication Repository of HZDR:

https://www.hzdr.de/publications/Publ-29011

Release of the secondary publication
on the basis of the German Copyright Law § 38 Section 4.

Check for updates

View Article Online
View Journal

Journal of Materials Chemistry C

Accepted Manuscript

This article can be cited before page numbers have been issued, to do this please use: R. Pushkarev, N. I. Fainer, V. Kirienko, A. Matsynin, V. A. Nadolinnyi, I. S. Merenkov, S. V. Trubina, S. B. Erenburg and K. Kvashnina, *J. Mater. Chem. C*, 2019, DOI: 10.1039/C9TC00299E.

This is an Accepted Manuscript, which has been through the Royal Society of Chemistry peer review process and has been accepted for publication.

Accepted Manuscripts are published online shortly after acceptance, before technical editing, formatting and proof reading. Using this free service, authors can make their results available to the community, in citable form, before we publish the edited article. We will replace this Accepted Manuscript with the edited and formatted Advance Article as soon as it is available.

You can find more information about Accepted Manuscripts in the author guidelines.

Please note that technical editing may introduce minor changes to the text and/or graphics, which may alter content. The journal's standard Terms & Conditions and the ethical guidelines, outlined in our author and reviewer resource centre, still apply. In no event shall the Royal Society of Chemistry be held responsible for any errors or omissions in this Accepted Manuscript or any consequences arising from the use of any information it contains.

ROYAL SOCIETY OF CHEMISTRY

rsc.li/materials-c

View Article Online
DOI: 10.1039/C9TC00299E

Journal Name

ARTICLE

SiC_xN_y:Fe films as a tunable ferromagnetic material with tailored conductivity†

Received 00th January 20xx,
Accepted 00th January 20xx

DOI: 10.1039/x0xx00000x

www.rsc.org/

Roman Pushkarev[a], Nadezhda Fainer[a], Victor Kirienko[b], Alexey Matsynin[c], Vladimir Nadolinnyy[a], Ivan Merenkov[a,d], Svetlana Trubina[a], Simon Ehrenburg[a,e], Kristina Kvashnina[f,g]

Amorphous ferromagnetic materials with the variable composition are promising candidates for application in rapidly-growing technological fields, such as spintronics. However, the significant downside of current state-of-art materials is a conductivity mismatch between injector and semiconductor which often is associated with the unavailability to control and precisely tailor magnetic properties and conductivity. We report on the synthesis of soft-magnetic SiC_xN_y:Fe films with the saturation magnetization of 20 e.m.u./cm^3 and conductivity similar to the one of Si, which is crucial for possible applications. XRD with synchrotron radiation and EXAFS revealed the complex composite structure of the films: crystals of Fe_3Si, Fe_5Si_3, SiC and graphite are embedded into the amorphous matrix of SiC_xN_y. The variation of deposition conditions allowed us to separately control the magnetic properties through the iron concentration and the conductivity of the material through the amorphous SiC_xN_y matrix composition. The reported results revealed a significant potential of SiC_xN_y:Fe films as a prospective object for analysis of spin-polarized transport in amorphous semiconductors and for application in field of spintronics.

Introduction

The development of new technology fields requires new materials with the wide variety of functional properties. The multi-functional materials are designed in a way, so one can tailor their properties by changing the composition, temperature, electromagnetic field, and etc. An exciting example of properties to combine is the ferromagnetism and semiconductivity. Tunable charge transfer properties combined with ferromagnetic ordering may solve existing problems in semiconductor spintronics and magnetic sensor materials. Different approaches were used in order to obtain the materials possessing the desired combination. One of the most widely investigated examples of magnetic semiconductors is ZnO or $A^{III}B^{V}$ doped with atoms of *d*-elements[1–6]. Despite the fact of achieving ferromagnetic ordering in these materials several problems, such as low Curie temperature (lower than room temperature) and limited solubility of metals in the semiconducting matrix, remains unsolved[7–9]. The control over ferromagnetic material conductivity is another essential task for spintronics. The contact resistance of spin injector is to be engineered at the optimum level, otherwise, the conductivity mismatch will result in the absence of spin-polarized current[10,11].

The ferromagnetic semiconductors with amorphous matrix are considered as the possible solution for these problems[12]. These materials possess properties, exceeding one of the crystal analogies. The subclass of ferromagnetic semiconductors with amorphous matrix is the granular systems, where magnetic particles are embedded into the amorphous matrix of the insulator. Magnetic metal particles combined with the insulator matrix gives the rise to the formation of a semiconducting composite with magnetic ordering[13,14]. Unfortunately, the goal to control the conductivity and magnetic properties of these composites in a precise way remains unsolved. The possible solution to this obstacle is the application of an amorphous matrix with variable composition, such as SiC_xN_y, instead of ones with the fixed stoichiometry. One can tune the conductivity of SiC_xN_y in a very wide range[15,16]. Through the variation of matrix conductivity, one can control the conductivity of composite material where magnetic iron-containing particles are embedded into the SiC_xN_y matrix. It will allow one to create ferromagnetic semiconductors or insulators, which is useful either for injection or detection of spin-polarized current[17,18].The tunable conductivity of ferromagnetic material is a useful tool for overcoming the conductivity mismatch problem[19].

The earlier reports devoted to the creation of magnetic materials based on the SiC_xN_y were focused on the ceramics[5], while the films and other low-dimensional materials are required for building of spintronics devices. Also, no information about the conductance of these composites, which is essential for spintronics, was provided.

[a] Nikolaev Institute of Inorganic Chemistry, Siberian Branch of Russian Academy of Sciences, Novosibirsk, pr. Acad. Lavrent'ev, 3, 630090, Russia.
[b] Rzhanov Institute of Semiconductor Physics, Siberian Branch of Russian Academy of Sciences, Novosibirsk, pr. Acad. Lavrent'ev, 13, 630090, Russia.
[c] Kirensky Institute of Physics, Siberian Branch of Russian Academy of Sciences, Krasnoyarsk, Akademgorodok 50, 38, 660036, Russia.
[d] Ural Federal University, Ekaterinburg, st. Mira, 19, 620002, Russia.
[e] Budker Institute of Nuclear Physics, Siberian Branch Russian Academy of Sciences, pr. Acad. Lavrent'ev, 11, Novosibirsk, 630090, Russia.
[f] Rossendorf Beamline at ESRF, 38043, Grenoble, France.
[g] HZDR, Institute of Resource Ecology, 01314, Dresden, Germany.
† Electronic Supplementary Information (ESI) available. See DOI: 10.1039/x0xx00000x

Published on 13 March 2019. Downloaded by JOINT ILL - ESRF LIBRARY on 3/19/2019 3:02:18 PM.

Journal of Materials Chemistry C Accepted Manuscript

Please do not adjust margins

View Article Online
DOI: 10.1039/C9TC00289E

Published on 13 March 2019. Downloaded by JOINT ILL - ESRF LIBRARY on 3/19/2019 3:02:18 PM.

Journal of Materials Chemistry C Accepted Manuscript

It is worth noting, that study conductivity mechanism and origin of ferromagnetism in these materials is of the essence for potential application in spintronics. Considerable advances in studying of these mechanisms were achieved for materials with the ordered crystal structure, such as diluted magnetic semiconductors based on ZnO and $A^{III}B^{V}$ compounds[20,21]. Still, this work is on-going and requires more efforts before the origin of room temperature ferromagnetism will be established[22]. The conductivity and ferromagnetism mechanisms are significantly less studied for materials with an amorphous structure. This work provides new insight into the electron transport and magnetic properties of complex materials with an amorphous structure. Presented results may become a basis for the more detailed study of spin-polarized transport mechanisms in amorphous semiconductors useful for spintronic technology.

Experimental part

Deposition procedure

The SiC_xN_y:Fe films were synthesized using a chemical vapor deposition technique by the thermal decomposition of three different gaseous mixture. Tris(diethylamino)silane (TDEAS) and ferrocene were used as sources of Si, C, N, and Fe, respectively and were common for all the mixtures. In order to tailor the composition of the films in a precise way, we used either helium, or hydrogen, or ammonia as the third component of gas mixture. The first one in an inert gas, while the other two may change the composition of the deposited films, e.g. in the SiC_xN_y synthesis procedures introduction of ammonia results in nitrogen concentration rising[23,24].

The deposition procedure was carried out in a horizontal quartz tube. The deposition conditions are described as follows: the deposition temperature range of 800-1000 °C, the partial pressure of components $P_{TDEAS} = 5\times10^{-2}$ Torr, $P_{Ferrocene} = 3\times10^{-2}$ Torr and $P_{gas} = 3\times10^{-2}$ Torr. The residual pressure was about $(7\text{-}8)\times10^{-4}$ Torr. The preliminary degreasing followed by chemical treatment in HF of the Si (100) wafers were used for all the specimens obtained.

Characterization methods

The microstructure of the surface of the film was studied by scanning electron JSM-6700F microscope with a resolution of 1 nm, and the elemental composition was examined by energy dispersive spectroscopy (EDS) with an EX-23000VU detector for this microscope. All the IR absorption spectra of the films were recorded on an FTIR SCIMITAR FTS 2000 spectrometer in the range 300—4000 cm^{-1}. The FTIR spectra were normalized to the film thickness and fitted with Gaussian profile function using Origin software. The Raman spectra were recorded using Triplemate, Spex spectrometer equipped with the argon ion laser with wavelength of 488 nm. The phase composition of the films was studied on the "Precision diffractometry and anomalous scattering" station of "Siberian Synchrotron and Terahertz Radiation Centre" (Novosibirsk, Russia) using Bragg-Brentano experimental geometry. The incident beam wavelength was set at 1.5410 Å.

The EXAFS (extended X-ray absorption fine structure) spectra of the SiC_xN_y:Fe films were measured at the BM20 beamline channel, ESRF, Grenoble, France. Plates with films were glued to a table and placed under a monochromatic synchrotron radiation beam at an angle of about 3º. The spectra were measured at Fe*K* absorption edge in the energy range 6867 – 8091 eV, which corresponds to the wavenumber k range up to 16 $Å^{-1}$ (X-ray Fe*K* absorption edge is 7112 eV). The spectra were measured under fluorescence conditions with a 12-channel Ge detector. Si(111) was used as a crystal-monochromator. Two mirrors with Rh coating were used to focus a beam in the horizontal and vertical planes. The quantum flux in recording spectra was approximately 7×10^{10} photons/s in a beam 200µm x 5mm in size. The local surroundings modelling was carried out using EXCURVE 98.

EPR spectra were recorded on the modified Varian E-109 spectrometer at 9.5 GHz and Bruker ELEXSYS 500 at 9.44 GHz. The 2,2-diphenyl-1-picrylhydrazyl (DPPH) and Mn^{2+} were used as *g*-factor standards, respectively.

Magnetic properties of the films were investigated with torque magnetometer. The procedure of the measurements is described elsewhere[25]. The equation

$$\Psi H/L = {}^{1}/_{M_s V} + {}^{H}/_{2K_{\perp} V},$$

where *L* is the torque moment, *H* – external magnetic field, M_s – saturation magnetization, *V* – specimen volume, $K_{\perp}$ - perpendicular anisotropy constant, is suitable in the case when the direction of the magnetic field applied to the specimen forms a small angle Ψ with the specimen plane. Studying the $\Psi H/L$ as a function of H allows one to determine a M_s and $K_{\perp}$. All measurements were carried at room temperature in the magnetic field range of 0 - 2000 Oe.

The I-V curves analysis of the Al/SiC_xN_y:Fe/Si structures allowed us to determine the conductivity of the SiC_xN_y:Fe films at room temperature. In order to create such a multilayer structure the Al was deposited as an electrode on the surface of SiC_xN_y:Fe/Si(100). The surface of Al electrode was 0.7×0.7 mm^2. Since the thickness of the films may vary due to the different deposition rates at various temperatures, the electric conductivity was determined at the electric field of 10^5 V/cm.

Results and discussion

Structure and morphology of SiC_xN_y:Fe films

This journal is © The Royal Society of Chemistry 20xx

Please do not adjust margins

View Article Online
DOI: 10.1039/C9TC00299E

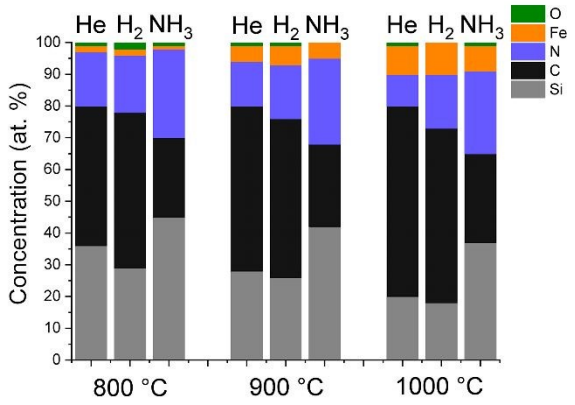

Fig. 1. Elemental composition of SiC_xN_y:Fe films deposited at different temperatures (denoted at the bottom) from gaseous mixtures, containing He, H_2 or NH_3

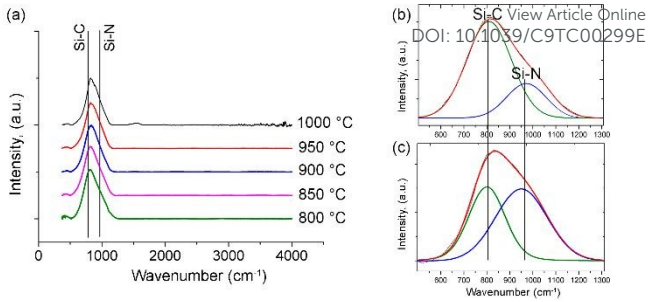

Fig. 2. (a) – FTIR spectra of SiC_xN_y:Fe films deposited from gaseous mixture of TDEAS, ferrocene, and helium at different temperatures, (b, c) – FTIR spectra (in the range of 500-1300 cm^{-1}) of SiC_xN_y:Fe films deposited from hydrogen and ammonia-containing gas mixtures, respectively

As it was mentioned earlier, the control over the functional properties of SiC_xN_y:Fe films is possible through the variation of structure and elemental composition. By changing the deposition temperature and gas phase composition we were able to synthesize films with different elemental composition as depicted on Fig. 1. In case of deposition from gaseous mixtures containing helium or hydrogen, the dominance of carbon in film composition is obvious. Elemental composition of the films obtained from the helium-containing mixture changes with the deposition temperature growing: carbon concentration grows from 45 at. % to 60 at. %, while silicon concentration becomes lower from 38 at. % to 20 at. % (Fig. 1). The nitrogen concentration remains approximately constant ~15 at. %. Deposition from a mixture of ferrocene, TDEAS, and hydrogen leads to the same tendencies for elemental composition vs. deposition temperatures. It is worth mentioning, that such a dominance of carbon in film composition may originate from the presence of free carbon phase[26]. The composition of the films deposited from the ammonia-containing mixture differs significantly from the composition of the films mentioned earlier. The main element, in this case, is the silicon with the concentration of 40-45 at. %. Nitrogen concentration is about 25-30 at. % which is significantly higher than for the films deposited from the helium or hydrogen-containing mixtures. The Fe concentration growth with the deposition temperature rising is the general tendency for all gaseous mixtures. Films deposited at 800 °C contain ~2-3 at. % of iron. Higher deposition temperatures allow one to obtain films containing up to 10 at % of iron. The variation of Fe concentration provides an opportunity to control the magnetic properties of the films. Oxygen presents in the films as an admixture with a concentration of 0-2 at. %.

Previous studies of amorphous SiC_xN_y indicated that this substance can be described as tetrahedral coordination of C and N atoms to Si atoms. Thus, structural fragments of Si-C-Si, Si-N-Si, and Si-C-C-Si is the main building blocks of amorphous SiC_xN_y[27–29]. According to this structure model, C-N bonds are absent in this material. Therefore, we assume that the structure of amorphous matrix of SiC_xN_y:Fe films are similar to one of SiC_xN_y films. This suggestion was confirmed by the **FTIR spectra** analysis of SiC_xN_y:Fe films (Fig. 2).

The common feature of FTIR spectra of SiC_xN_y:Fe films deposited in this work is the asymmetric peak with a maximum at 850 cm^{-1}. This broad peak consists of two components related to the vibration of Si-C and Si-N bonds centered at 800 and 950 cm^{-1}, respectively (Fig. 2a). As one can see, peaks of C-N related fragments are absent. We concluded that the amorphous part of the material has a structure similar to the one of SiC_xN_y described earlier: Si atoms with C and N tetrahedral coordination.

In order to compare the FTIR spectra of the films deposited in different experimental conditions (e.g., deposition temperature, gaseous mixture composition) its intensity were divided on the film thickness. Since the broad peak intensity does not depend on the deposition temperature, we concluded that the composition of SiC_xN_y matrix does not depend on the deposition temperature. Therefore, it can be concluded, that rising concentration of carbon with growing deposition temperature promotes the formation of free carbon phase. The small peak around 1500 cm^{-1} emerging in case of deposition at 1000°C can be attributed to the disordered graphite phase. The appearance of this peak is in agreement with the above-mentioned conclusion. Due to limitations of the FTIR method for analysis of carbon-containing phases, Raman spectroscopy is required to study the formation of disordered graphite in more detail. The most interesting tendency in FTIR spectra is observed for intensity ratio $I_{Si\text{-}C}/I_{Si\text{-}N}$. This ratio changes with the gas mixture composition being varied. The deposition from a gas mixture of ferrocene, TDEAS and helium results in $I_{Si\text{-}C}/I_{Si\text{-}N}$ = 2.4-2.5. Such Si-C bond dominance in FTIR spectra of SiC_xN_y films synthesized by CVD technique at temperatures higher than 400

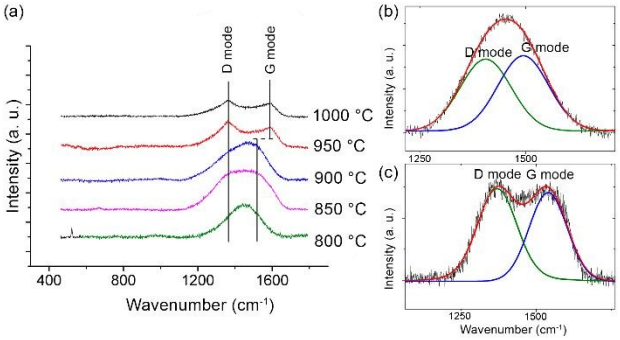

Fig. 3. (a) - Raman spectra of SiC_xN_y:Fe films deposited from gaseous mixture of TDEAS, ferrocene, and helium, (b, c) - detailed Raman spectra of the films deposited at 800°C and 1000°C, respectively

Published on 13 March 2019. Downloaded by JOINT ILL - ESRF LIBRARY on 3/19/2019 3:02:18 PM.

Journal of Materials Chemistry C Accepted Manuscript

Please do not adjust margins

View Article Online
DOI: 10.1039/C9TC00305F

Published on 13 March 2019. Downloaded by JOINT ILL - ESRF LIBRARY on 3/19/2019 3:02:18 PM.

Journal of Materials Chemistry C Accepted Manuscript

°C was mentioned earlier by Wrobel[30–32]. While the substitution of helium for hydrogen does not affect the intensity ratio (Fig. 2b), deposition from ammonia-containing mixture results in the formation of films with the Si-N bond vibration peak having similar intensity to the one of Si-C peak (Fig. 2c). The ratio of $I_{Si\text{-}C}/I_{Si\text{-}N}$, in this case, is significantly lower (0.7-0.8). This change indicates that the structure of amorphous SiC_xN_y matrix changes from the one close to amorphous SiC_x to the one enriched with Si-N bonds similar to amorphous SiN_x. We assume that control over the amorphous matrix composition will provide us an opportunity to change functional properties of the material (e.g. relative conductivity).

As it was mentioned, in the case of helium and hydrogen-containing mixtures carbon is the main element of the films. The excessive C concentration leads to the formation of free carbon phases such as amorphous carbon and graphite which was confirmed by **Raman spectroscopy**. Raman spectra of SiC_xN_y:Fe films (Fig. 3a) contain two main peaks: D and G modes related to the different state of carbon phase[33]. The relative intensity and position of the D and G modes provide valuable information about the structure of carbon spices. In case of the films deposited from helium-containing mixture in the temperature range of 800-900 °C the D mode is centered at ~1360 cm^{-1}, while the G mode center positioned at 1520 cm^{-1} (Fig. 3b). The position of the peaks combined with the relative intensity of I_D/I_G = 1-1.5 allows us to conclude that the majority of free carbon exists in an amorphous form. Deposition at higher temperatures results in a shift of the G mode center to higher wavenumber (1580 cm^{-1}) which is an evidence of carbon graphitization (Fig. 3c). This tendency for graphitization at elevated temperatures is well known and may influence the electrical conductivity of the films. Raman spectra of SiC_xN_y:Fe films deposited from hydrogen-containing mixtures also have the same D and G modes, but the shift of the latter one to higher wavenumbers occurs at higher temperature of 1000 °C. Thus, the hydrogen slightly influences the carbon phase composition and has almost no effect on SiC_xN_y matrix. In case of deposition using ammonia-containing gas mixture Raman spectra are less intense, which outlines the lower carbon concentration. In addition, G mode center shifts to higher wavenumbers at the same deposition temperature as in the case of the hydrogen-containing mixture. Thus, the variation of the gas mixture composition by changing helium for hydrogen or ammonia provides us an opportunity to control free carbon phase composition in SiC_xN_y:Fe films.

Morphology of 2D materials, such as films, is a crucial parameter which may have a great influence on its functional properties. The surface of the films deposited from 3 gaseous mixtures changes similarly with the deposition temperature growing. The morphology of the films deposited in the temperature range of 800-1000 °C with the ΔT = 50 °C from helium-containing mixture depicted in the Fig. 4. Deposition at 800 °C leads to the formation of the surface similar to one of the amorphous SiC_xN_y films. At this temperature, the rate of ferrocene decomposition is low compared to the decomposition rate (DR) of TDEAS. As it was mentioned earlier, the concentration of iron does not exceed 3 at. %. Elevation of deposition temperature up to 850 °C and higher exerts the ferrocene decomposition with the rate sufficient to reach iron atoms concentration in film up to 10 at. %. Morphology of the films obtained at 900 °C has a globule-like structure. As one can see, the surface of the films deposited at 850 °C is composed of nuclei of the globules which precedes the formation of the morphology of the films synthesized at 900 °C. Further deposition temperature elevation results in higher iron concentration and formation of small grains on the film surface with the size of 50-70 nm, while the size of globules obtained in case of deposition at 900 °C varies in the range of 0.5 – 4 μm.

Formation of globe-like structures can be described with a model of "core-shell" structure where the core is the nucleus of the crystal phase and the shell is represented by an amorphous substance. It was shown in our previous work[34], that the formation of crystallite inside the amorphous matrix begins at temperatures around 900 °C making the scenario of "core-shell" structure formation possible. The similar results were earlier mentioned for different carbides, nitrides, and carbon materials[35–41]. At higher deposition temperatures, the DR of ferrocene is much higher resulting in the formation of a large number of crystal nuclei. Therefore, the surface of films deposited above 900 °C has granular-like structure.

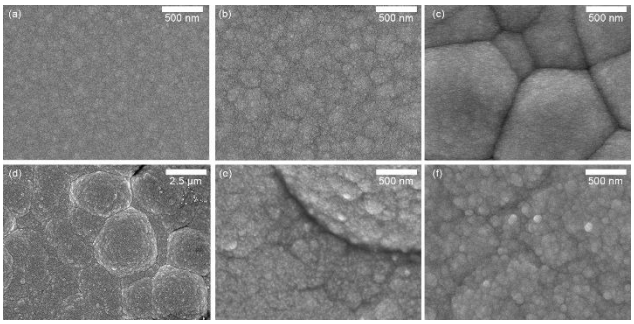

Fig. 4. Surface morphology of SiC_xN_y:Fe films deposited from gaseous mixture of TDEAS, ferrocene, and helium at (a) – 800°C, (b) – 850°C, (c) – 900°C, (d,e) – 950°C, (f) – 1000°C

In order to study the structure of the films in more detail, we used **XRD with a synchrotron radiation** source. Conventional X-ray diffractometers do not provide sufficient beam brightness making it difficult to analyze the composition of composite films with small crystallites. The SiC_xN_y:Fe films deposited at temperatures lower than 900 °C has an amorphous structure with no significant amount of crystallites inclusions (Fig. 5a). At higher deposition temperatures formation of Fe_5Si_3, Fe_3Si, FeSi, β-SiC, and graphite crystallites occur (Fig. 5b). Unfortunately, it is difficult to conduct qualitative analysis due to the fact that the major peak at 45° can be attributed to both FeSi and Fe_5Si_3 phases. Therefore, additional structure analysis is required.

It is worth to mention, that the deposition of SiC_xN_y in the same condition without the introduction of ferrocene leads to the formation of amorphous films without any crystallites embedded into an amorphous matrix[42]. Therefore, we

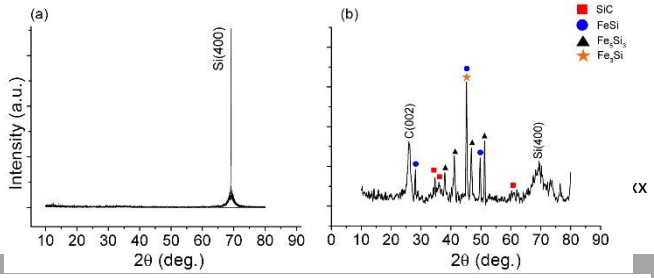

Fig. 5. XRD pattern of SiC_xN_y:Fe films deposited from gaseous mixture of TDEAS, ferrocene, and helium at (a) – 800°C, (b) – 1000°C

Please do not ad

View Article Online
DOI: 10.1039/C9TC00299E

Published on 13 March 2019. Downloaded by JOINT ILL - ESRF LIBRARY on 3/19/2019 3:02:18 PM.

concluded that the formation of iron-containing spices serves as a driving force for the silicon carbide and carbon crystallization. This phenomenon could be described with the formation of Fe-Si-C solid solution, which promotes the crystallization of crystallites composed of light elements, such as Si and C[43].

Non-equilibrium nature of the CVD process and the local equilibrium is the reason why the mixture of silicides is formed. The phase diagram of Fe-Si system has a field of Fe_3Si and Fe_5Si_3 coexistence in the temperature region of 800-1000 °C. Moreover, there is a field of Fe_5Si_3 and FeSi coexistence in the same temperature region with slightly more silicon concentration. The existence of this phase field might be the reason for the formation of different iron silicides. Also, such a variety of silicides is possible due to their interconversion, described earlier[44].

Due to the presence of multiple iron-containing phases, it is necessary to conduct additional analysis in order to establish which phase is dominant. **EXAFS** was used as a tool for analysis of the films deposited from the helium- and ammonia-containing gas mixture. The modules of Fourier transform magnitudes |F(R)| for experimental Fe*K* EXAFS spectra of SiC_xN_y:Fe films are presented in the Fig. 6. One can see that the spectrum of the film deposited from He-containing mixture differs significantly from the one deposited from NH_3-containing mixture. The higher intensities in case of the former one reveal its better crystallinity. According to XRD of the sample deposited from He-containing mixture it contains FeSi, Fe_3Si, Fe_5Si_3 in unknown concentrations. The analysis of local environment of iron atoms in this film pointed out the dominance of Fe_3Si phase (interatomic distances in 1st coordination sphere R(Fe-Fe)=2.48 Å; R(Fe-Si)=2.83 Å) with the concentration ~60 %, while the FeSi (interatomic distances in 1st coordination sphere R(Fe-Fe)=2.76 Å; R(Fe-Si)=2.35 Å) has the concentration of ~30%. These results allow us to conclude that Fe_5Si_3 has rather low concentration of even absent in this case. The analysis of the film deposited from NH_3-containing mixture revealed the dominant concentration of Fe_5Si_3 phase with the interatomic distances of R(Fe-Si)=2.35 Å; R(Fe-Fe)=2.36; Å; R(Fe-Fe)=2.85 Å. The presence of Fe_3Si and Fe_5Si_3 crystals stipulates ferromagnetic properties of SiC_xN_y films, but the reason behind the crystal composition changing yet remains unclear. The possible explanation for the coexistence of different silicides was given earlier, but their interconversion is a question of further study. The answer to this question may provide and efficient tool to control phase composition of iron silicides and, therefore, magnetic properties of SiC_xN_y:Fe films in a very precise way.

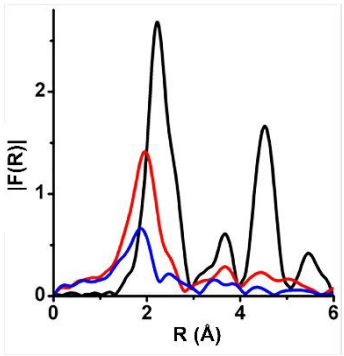

Fig. 6. Modules of Fourier transform magnitudes |F(R)| for experimental Fe*K* EXAFS spectra of SiC_xN_y:Fe films deposited from gaseous mixture of TDEAS, ferrocene, and helium at 1000°C (red line), or NH_3 at 1000°C (blue line), and reference Fe foil (black line).

EPR was used to carry out a general analysis of magnetic ordering in SiC_xN_y:Fe films. EPR spectra of the film deposited at 850 °C from helium-containing mixture has one broad peak with g-factor 2.056 (Fig. 7). This value indicates the existence of paramagnetic centers with an electron spin s = 1/2. According to earlier research[45], this signal may be assigned to Fe^{3+} embedded into the amorphous matrix of silicon carbonitride. According to EDS analysis, the iron concentration in films deposited in the temperature interval of 800-900 °C is about 2-3 at. %. In these conditions formation of iron-containing crystallites is unfavorable, thus, iron exists as an Fe^{3+} ion distributed in the amorphous SiC_xN_y matrix. The absence of crystal phases of any kind which may possess paramagnetic properties was confirmed by XRD with synchrotron radiation. Also, it is worth noting, that undoped SiC_xN_y films deposited from the mixture of TDEAS and helium also possesses paramagnetic resonance with significantly lower intensity. It may be due to the formation of dandling bonds in amorphous matrix or existence of small crystals (<5 nm) of defective graphite[46]. Still, the iron-doped films have EPR signal with higher intensity when the iron concentration is about 2-3 at. %. Qualitative analysis of EPR spectra of the film deposited at 900 °C pointed out the ferromagnetic nature of the specimen. The signal with g = 9.9 relates to ferromagnetic resonance which originates from iron-containing phases. The formation of FeSi crystallites starts in these conditions. According to the phase diagram of Fe-Si binary system[43] at temperatures close to 900 °C FeSi may coexist with Fe_5Si_3, which is ferromagnetic[47]. Moreover, FeSi itself may possess ferromagnetic properties while exists in nanocrystallite state[48,49]. The signal with g ~ 2 still presents, but its intensity is lower than the one of signal described above. When the deposition temperature is elevated to 1000 °C, the intensity of the signal with g ~ 2 becomes negligible compared to the signal with g = 9.9. The formation of ferromagnetic phases, in this case, was confirmed by XRD and EXAFS analysis. The similar tendencies were observed for gaseous mixtures containing hydrogen or ammonia.

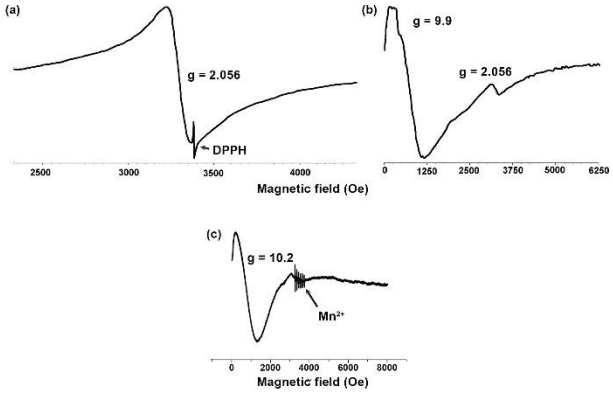

Fig. 7. EPR spectra of SiC_xN_y:Fe films deposited from gaseous mixture of TDEAS, ferrocene, and helium at (a) – 800°C, (b) – 900°C, (c) – 1000 °C

Journal of Materials Chemistry C Accepted Manuscript

View Article Online
DOI: 10.1039/C9TC00299E

Published on 13 March 2019. Downloaded by JOINT ILL - ESRF LIBRARY on 3/19/2019 3:02:18 PM.

Journal of Materials Chemistry C Accepted Manuscript

Functional properties of SiC_xN_y:Fe films

More detailed analysis of **magnetic properties** was carried out using vibration magnetometer technique. Fig. 8 represents the magnetization vs. magnetic field dependencies for the SiC_xN_y:Fe films deposited in the temperature range of 900-1000 °C. The saturation magnetization for ferromagnetic films deposited at temperatures of 900 °C and higher grows with the deposition temperature rising. Films deposited at temperatures lower than 900 °C do not possess ferromagnetic properties due to the low iron concentration and absence of ferromagnetic phase. Low iron concentration results in low magnetization values below detection threshold. The coercivity of ferromagnetic films deposited above 900 °C does not exceed 20 Oe, making these films soft-magnetic materials. The value of 20 Oe is in an agreement with previously reported coercivity for nano-sized Fe_5Si_3 and Fe_3Si phases[47]. Curie temperature of the sample containing Fe_5Si_3 is close to 400 K which is higher than room temperature[50], which makes this material promising for spintronic applications. Table 1 summarizes the saturation magnetization of the SiC_xN_y:Fe films synthesized in different conditions. One can see, that the tendencies of magnetization changing are general for all gas mixtures: the magnetization grows with the deposition temperature rising.

Thus, it can be concluded, that iron silicide phases formed in the composite material is the main reason of the ferromagnetic properties of the films. Despite the fact of different iron atoms distribution between iron silicides in case of deposition from He- and NH_3-containing mixtures the magnetic properties of the films remains similar. This fact is due to the similar magnetic properties of Fe_5Si_3 and Fe_3Si phases. The saturation magnetization of latter one is higher than the one of Fe_5Si_3, but overall magnetization of the films is the same due to lower concentration of Fe_3Si phase as it was shown with EXAFS. The saturation magnetization of SiC_xN_y:Fe films are close to one of the materials based on ZnO and $A^{III}B^{V}$ compounds making SiC_xN_y:Fe films an interesting and promising material for further study.

The material **conductivity** is another important parameter for the creation of a ferromagnetic semiconductor. The detailed analysis of undoped SiC_xN_y film conductivity was carried out by different authors[51,52]. Summarizing these data, the following tendencies can be outlined:

1. With the deposition temperature raising the SiC_xN_y film conductivity tends to grow due to variable range hopping mechanism which comes into actions with the formation of crystals of SiC and Si_3N_4.
2. The carbon concentration growth leads to the formation of free carbon phase, which exists as an amorphous one or as a graphite crystal. The latter ones possess larger conductivity compared to the amorphous matrix.
3. The nitrogen concentration growth results in the formation of highly defective carbon phase with the structure similar to the amorphous one. Thus, the conductivity of SiC_xN_y films lowers with N concentration rising.

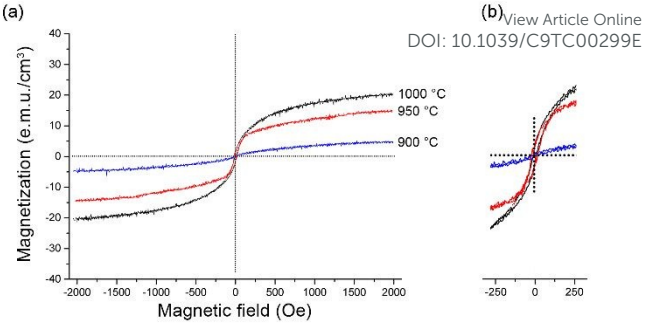

Fig. 8. (a) - magnetization curves of the SiC_xN_y:Fe films deposited at 900-1000 °C from He-containing gas mixture, (b) – magnetization curves in -250-250 Oe magnetic field range

Obviously, the Fe-doping of SiC_xN_y films may change the charge transfer mechanism. The electrical conductivity of SiC_xN_y:Fe films vs. deposition temperature for different gaseous mixtures are summarized in Table 1.

The following statements describe the observed tendencies:

1. The conductivity of SiC_xN_y films doped with Fe is higher than one of the undoped films. The formation of iron-containing species gives the rise to new charge transfer mechanisms, such as variable range hopping, typical for systems of insulator matrix with embedded metal clusters.
2. SiC_xN_y:Fe films deposited at 1000 °C possesses the highest conductivity among all of the samples due to the high iron concentration up to 10 at. % and formation of iron silicide crystal phases such as, Fe_5Si_3 and FeSi, which has higher conductivity than amorphous SiC_xN_y.
3. Substitution of helium for hydrogen or ammonia results in conductivity decreasing. The composition of amorphous matrix changes significantly from the one enriched with carbon, to the one, close to SiN_x.

The conductivity of SiC_xN_y:Fe films may be changed in a very wide range from 10^{-12} to 6.9×10^{-4} S/cm. However, the films deposited below 900 °C are paramagnetic and have no prospective application for spintronics. For the ferromagnetic films deposited in the temperature range of 900-1000 °C the conductivity can be tuned 1.6×10^{-7}-6.9×10^{-4} S/cm, which stands for more than 3 orders of magnitude. Moreover, the conductivity of the films deposited at 1000 °C may vary from 2.0×10^{-5} to 6.9×10^{-4} S/cm, while their saturation magnetization

Table 1. Conductivity and saturation magnetization of SiC_xN_y:Fe films deposited in the temperature range of 800-1000 °C

Additional gas	Deposition temperature, °C	Conductivity, S/cm	Saturation magnetization, e.m.u./cm³
He	800	4.3×10^{-5}	
	900	3.6×10^{-4}	5±1
	1000	6.9×10^{-4}	20±2
H_2	800	1.6×10^{-6}	
	900	3.6×10^{-6}	5±1
	1000	2.0×10^{-4}	18±2
NH_3	800	10^{-12}	
	900	1.6×10^{-7}	5±1
	1000	2.0×10^{-5}	20±2

This journal is © The Royal Society of Chemistry 20xx

Please do not adjust margins

View Article Online
DOI: 10.1039/C9TC00495E

Published on 13 March 2019. Downloaded by JOINT ILL - ESRF LIBRARY on 3/19/2019 3:02:18 PM.

Journal of Materials Chemistry C Accepted Manuscript

and coercivity remain constant. These films have the highest saturation magnetization among all of the obtained SiC_xN_y:Fe films. This fact combined with the conductivity being similar to the one of Si makes this material a promising candidate for the creation of spin injector into silicon. The substitution of helium for hydrogen or ammonia results in a lower conductivity of the films, which may be useful for creation of spin-polarized current detector. One can conclude, that it is possible to tailor the transport properties of the material through the variation of amorphous matrix composition without any change of its magnetic properties. This fact can be considered as a significant advantage when SiC_xN_y:Fe films are compared to other ferromagnetic semiconductors. The saturation magnetization and Curie temperature of *d*-metal doped ZnO are lower than the ones of SiC_xN_y:Fe films[7–9]. Application of ferromagnetic material based on $(Bi,Sb)_2Te_3$ with tunable conductivity are limited due to low Curie temperature[18]. The promising ferromagnetic semiconductor $Co_{28.6}Fe_{12.4}Ta_{4.3}B_{8.7}O_{46}$ with variable conductivity and properties exceeding other materials[12] were obtained in a bulk form, while the thin film materials are required for spintronic applications.

Unfortunately, the mechanism of charge transfer in SiC_xN_y:Fe films is studied insufficiently and remains an important question for future research. In the similar systems of dielectric matrixes, e.g. Ca-F, Al-O, with inclusions of metal particles the mechanism of electron transport is often represented as a variable range hopping (VRH) between metallic particles. One can assume that the conductivity of the SiC_xN_y:Fe films follow the similar pattern. Still, this assumption is to be confirmed for better understanding and more precise control of functional properties of SiC_xN_y:Fe films.

Conclusions

Ferromagnetic films SiC_xN_y:Fe with variable composition were synthesized using CVD technique. Thorough structure analysis revealed the composite nature of the material: Fe_3Si, Fe_5Si_3, SiC, and graphite crystals are embedded into the amorphous SiC_xN_y matrix. The variation of deposition temperature allowed us to change the iron concentration from 0 to 10 at. %. As a consequence, we can control the saturation magnetization of the film, making it as high as 20 e.m.u./cm^3. The saturation magnetization of the SiC_xN_y:Fe films may be improved through the elevation of iron concentration. The approach should be studied carefully due to the possible influence of higher ferrocene concentration on the phase composition. Currently, the low coercivity of 20 Oe related to the presence of iron silicides indicates that the films are soft-magnetic. The analysis of magnetic properties of SiC_xN_y:Fe films revealed that films deposited at 1000 °C possess the highest saturation magnetization, which can be useful for further spin-polarized charge-transfer research and application in the spintronics field. The interconversion of iron silicides discovered by EXAFS analysis may provide and effective tool to control magnetic properties in a very precise way, but this promising direction of this work is yet to be studied. The variation of gas phase composition is a useful tool to control SiC_xN_y matrix composition. With the substitution of helium for hydrogen and ammonia the conductivity of the films changes from 6.9×10^{-9} to 10^{-12} S/cm. The conductivity of the ferromagnetic films can be changed for 3 orders of magnitude, providing an opportunity to tailor properties in a wide range. It should be noted, that while the conductivity of the films changing, saturation magnetization and coercivity remain constant. Magnetic characteristics of the films deposited at 1000 °C combined with the conductivity close to the one of Si make these films promising material for further analysis of spin-polarized charge transfer. The study of spin injection processes from SiC_xN_y:Fe films to Si may provide insights useful for the spintronics field and reveal tendencies, which will shed some light of the transfer mechanism in amorphous semiconductors.

Conflicts of interest

There are no conflicts to declare.

Acknowledgements

This research did not receive any specific grant from funding agencies in the public, commercial, or not-for-profit sectors.

Notes and references

1 V. Sverdlov and S. Selberherr, *Phys. Rep.*, 2015, **585**, 1–40.
2 G. A. Prinz, *Phys. Today*, 1995, **48**, 58–63.
3 T. Nie, in *Reference Module in Materials Science and Materials Engineering*, Elsevier, 2016, pp. 1–5.
4 D. D. Awschalom and M. E. Flatté, *Nat. Phys.*, 2007, **3**, 153–159.
5 S. I. Andronenko and S. K. Misra, *Appl. Magn. Reson.*, 2015, **46**, 693–707.
6 M. Bououdina, Y. Song and S. Azzaza, *Nano-Structured Diluted Magnetic Semiconductors*, Elsevier Ltd., 2016.
7 Y. Köseoğlu, *Ceram. Int.*, 2015, **41**, 11655–11661.
8 D. Saikia and J. P. Borah, *J. Mater. Sci. Mater. Electron.*, 2017, **28**, 8029–8037.
9 Q. Mahmood, M. Hassan and M. A. Faridi, *Chinese Phys. B*, 2017, **26**, 027503.
10 A. Fert, *Angew. Chemie Int. Ed.*, 2008, **47**, 5956–5967.
11 Y. Yang, Z. Wu, W. Yang, J. Li, S. Chen and C. Li, *Appl. Phys. Express*, 2017, **10**, 063001.
12 W. Liu, H. Zhang, J. A. Shi, Z. Wang, C. Song, X. Wang, S. Lu, X. Zhou, L. Gu, D. V. Louzguine-Luzgin, M. Chen, K. Yao and N. Chen, *Nat. Commun.*, 2016, **7**, 13497.
13 N. Kobayashi, H. Masumoto, S. Takahashi and S. Maekawa, *Nat. Commun.*, 2014, **5**, 4417.
14 T. N. Koltunowicz, P. Zukowski, V. Bondariev, J. A. Fedotova and A. K. Fedotov, *Vacuum*, 2015, **120**, 44–50.
15 N. I. Fainer, M. L. Kosinova, Y. M. Rumyantsev, E. A. Maximovskii and F. A. Kuznetsov, *J. Phys. Chem. Solids*, 2008, **69**, 661–668.
16 N. I. Fainer, M. L. Kosinova, Y. M. Rumyantsev, E. A. Maksimovskii, F. A. Kuznetsov, V. G. Kesler, V. V. Kirienko,

Please do not adjust margins

B. S. Han and C. Lu, *Glas. Phys. Chem.*, 2005, **31**, 427–432.

17 E. Arias-egido, M. A. Laguna-marco, C. Piquer and R. Boada, 2019, **1806754**, 10–15.

18 Y. Ou, C. Liu, L. Zhang, Y. Feng, G. Jiang, D. Zhao, Y. Zang, Q. Zhang, L. Gu, Y. Wang, K. He, X. Ma and Q. Xue, *APL Mater.*, 2016, **4**, 086101.

19 S. Omar and B. J. van Wees, *Phys. Rev. B*, 2017, **95**, 081404.

20 A. Bouravleuv, V. Sapega, V. Nevedomskii, A. Khrebtov, Y. Samsonenko, G. Cirlin and V. Strocov, *J. Cryst. Growth*, 2017, **468**, 680–682.

21 M. Zhong, M. Zhu, Z. Zhang, M. Zhong, M. Tariq, Y. Li, W. Li, H. Jin, K. Skotnicova and Y. Li, *Ceram. Int.*, 2016, **43**, 3166–3170.

22 A. K. Rana, Y. Kumar, P. Rajput, S. N. Jha, D. Bhattacharyya and P. M. Shirage, *ACS Appl. Mater. Interfaces*, 2017, **9**, 7691–7700.

23 E. Ermakova, Y. Rumyantsev, A. Shugurov, A. Panin and M. Kosinova, *Appl. Surf. Sci.*, 2015, **339**, 102–108.

24 E. Tomasella, F. Rebib, M. Dubois, J. Cellier and M. Jacquet, *J. Phys. Conf. Ser.*, 2008, **100**, 082045.

25 S. Chikazumi, *J. Appl. Phys.*, 1961, **32**, S81.

26 Y. Wang, T. Jiang, L. Zhang and L. An, *J. Am. Ceram. Soc.*, 2009, **92**, 1603–1606.

27 P. Hoffmann, O. Baake, B. Beckhoff, W. Ensinger, N. Fainer, A. Klein, M. Kosinova, B. Pollakowski, V. Trunova, G. Ulm and J. Weser, *Nucl. Instruments Methods Phys. Res. Sect. A Accel. Spectrometers, Detect. Assoc. Equip.*, 2007, **575**, 78–84.

28 P. S. Hoffmann, N. I. Fainer, O. Baake, M. L. Kosinova, Y. M. Rumyantsev, V. A. Trunova, A. Klein, B. Pollakowski, B. Beckhoff and W. Ensinger, *Thin Solid Films*, 2012, **520**, 5906–5913.

29 B. Doucey, M. Cuniot, R. Moudni, F. Ténégal, J. E. Bourée, D. Imhoff, M. Rommeluére and J. Dixmier, *J. Mater. Sci.*, 2002, **37**, 2737–2745.

30 A. M. Wrobel, I. Blaszczyk-Lezak, P. Uznanski and B. Glebocki, *Plasma Process. Polym.*, 2011, **8**, 542–556.

31 A. M. Wrobel, I. Blaszczyk-Lezak, P. Uznanski and B. Glebocki, *Chem. Vap. Depos.*, 2010, **16**, 211–215.

32 N. I. Fainer, A. G. Plekhanov, A. N. Golubenko, Y. M. Rumyantsev, V. I. Rakhlin, E. A. Maximovski and V. R. Shayapov, *ECS J. Solid State Sci. Technol.*, 2014, **4**, N3153–N3163.

33 A. C. Ferrari, *Solid State Commun.*, 2007, **143**, 47–57.

34 R. V. Pushkarev, N. I. Fainer and K. K. Maurya, *Superlattices Microstruct.*, 2017, **102**, 119–126.

35 Q. G. Fu, H. J. Li, X. H. Shi, K. Z. Li, J. Wei and Z. B. Hu, *Mater. Chem. Phys.*, 2006, **100**, 108–111.

36 S. M. Manakov and T. I. Taurbayev, *J. Nanoelectron. Optoelectron.*, 2012, **7**, 619–622.

37 C. J. Oliphant, C. J. Arendse, G. F. Malgas, D. E. Motaung, T. F. G. Muller, S. Halindintwali, B. A. Julies and D. Knoesen, *J. Mater. Sci.*, 2009, **44**, 2610–2616.

38 P. Mahanandia, P. N. Viswakarma, P. V. Bhotla, S. V. Subramanyam and K. K. Nanda, *Bull. Mater. Sci.*, 2010, **33**, 215–220.

39 V. Prasad and S. V. Subramanyam, *Phys. B Condens. Matter*, 2005, **369**, 168–176.

View Article Online
DOI: 10.1039/C9TC00299E

40 A. Dasgupta, P. A. Premkumar, F. Lawrence, L. Houben, P. Kuppusami, M. Luysberg, K. S. Nagaraja and V. S. Raghunathan, *Surf. Coatings Technol.*, 2006, **201**, 1401–1408.

41 H. Cao, G. Huang, S. Xuan, Q. Wu, F. Gu and C. Li, *J. Alloys Compd.*, 2008, **448**, 272–276.

42 N. I. Fainer, A. N. Golubenko, Y. M. Rumyantsev, V. G. Kesler, E. A. Maximovskii, B. M. Ayupov and F. A. Kuznetsov, *Glas. Phys. Chem.*, 2013, **39**, 77–88.

43 J. Lacaze and B. Sundman, *Metall. Trans. A*, 1991, **22**, 2211–2223.

44 A. L. Schmitt, J. M. Higgins, J. R. Szczech and S. Jin, *J. Mater. Chem.*, 2010, **20**, 223–235.

45 T. Nakayamada, K. Matsuo, Y. Hayashi, A. Izumi and Y. Kadotani, *Thin Solid Films*, 2008, **516**, 656–658.

46 T. Shinjo, Y. Nakamura and N. Shikazono, *J. Phys. Soc. Japan*, 1963, **18**, 797–801.

47 M. K. Kolel-Veetil and T. M. Keller, *Materials (Basel).*, 2010, **3**, 1049–1088.

48 M. Strečková, J. Füzer, L. Kobera, J. Brus, M. Fáberová, R. Bureš, P. Kollár, M. Lauda, Ľ. Medvecký, V. Girman, H. Hadraba, M. Bat'Ková and I. Bat'Ko, *Mater. Chem. Phys.*, 2014, **147**, 649–660.

49 S. W. Hung, T. T. J. Wang, L. W. Chu and L. J. Chen, *J. Phys. Chem. C*, 2011, **115**, 15592–15597.

50 Y. Jing, J. Liu, W. Ji, W. Wang, S. He, X. Jiang, T. Wiedmann, C. Wang and J. Wang, *ACS Appl. Mater. Interfaces*, 2015, **7**, 12649–12654.

51 N. I. Fainer, M. L. Kosinova, Y. M. Rumyantsev, E. A. Maximovskii and F. A. Kuznetsov, *J. Phys. Chem. Solids*, 2008, **69**, 661–668.

52 B. Ma, Y. Wang, K. Wang, X. Li, J. Liu and L. An, *Acta Mater.*, 2015, **89**, 215–224.

Published on 13 March 2019. Downloaded by JOINT ILL - ESRF LIBRARY on 3/19/2019 3:02:18 PM.

Journal of Materials Chemistry C Accepted Manuscript

This journal is © The Royal Society of Chemistry 20xx

Please do not adjust margins

View Article Online
DOI: 10.1039/C9TC00299E

Published on 13 March 2019. Downloaded by JOINT ILL - ESRF LIBRARY on 3/19/2019 3:02:18 PM.

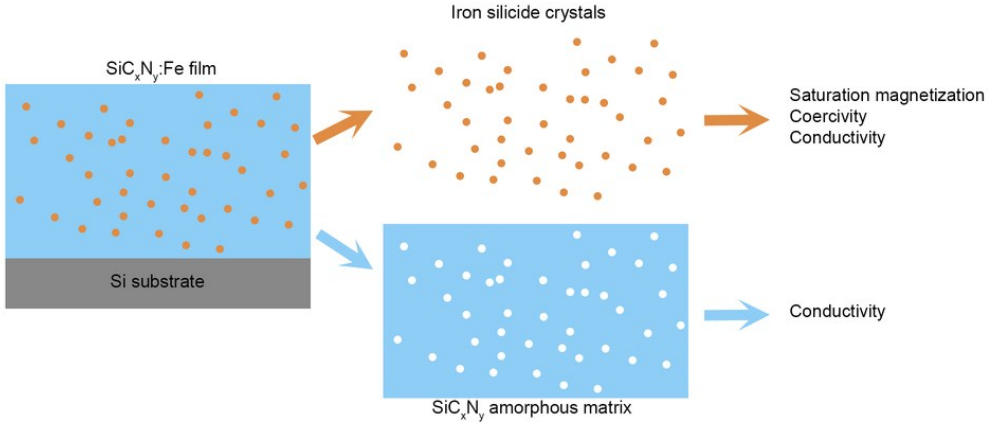

80x34mm (300 x 300 DPI)

Journal of Materials Chemistry C Accepted Manuscript

Ferromagnetic SiC_xN_y:Fe films with tunable functional properties were synthesized, providing a novel material for spintronic applications.

View Article Online
DOI: 10.1039/C9TC00299E

Published on 13 March 2019. Downloaded by JOINT ILL - ESRF LIBRARY on 3/19/2019 3:02:18 PM.

Journal of Materials Chemistry C Accepted Manuscript